Investigations on the Mechanisms of Ionic Conductivity in PEO−PU/PAN Semi-interpenetrating Polymer Network−Salt Complex Polymer Electrolytes: An Impedance Spectroscopy Study†

Pratyay Basak and Sunkara V. Manorama*

Materials Science Group, Inorganic and Physical Chemistry Division, Indian Institute of Chemical Technology, Hyderabad 500 007, India

Rajnish K. Singh and Om Parkash

Department of Ceramic Engineering, Institute of Technology, Banaras Hindu University, Varanasi 221 005, India

Received: August 31, 2004; In Final Form: November 8, 2004

This paper is a first comprehensive study on the correlated ion transport mechanisms contributing to the overall conductivity behavior in a new class of poly(ethylene oxide)−polyurethane/polyacrylonitrile (PEO−PU/PAN) semi-interpenetrating polymer networks (semi-IPNs)−salt complex polymer electrolytes. A simultaneous investigation of the electrical response on PEO−PU/PAN/$LiClO_4$ and PEO−PU/PAN/$LiCF_3SO_3$ semi-IPNs with varying EO/Li mole ratios (100, 60, 30, 20, 15, 10) has been carried out by impedance spectroscopy. Analysis of the complex plane and spectroscopic plots indicated the presence of two microscopic phases corresponding to the PEO−PU and PAN domains, which leads to space charge polarization in these systems. A suitably modified approach based on the universal power law (UPL) considering the independent contribution from the individual microphases of semi-IPNs facilitates a complete interpretation of the spectroscopic profiles for the real component of conductivity ($\sigma'(\omega)$). The $\sigma'(\omega)$ spectroscopic profiles were fitted with two power law equations, where the frequency region up to ∼300 kHz is the conductivity profile associated with the PAN phase and beyond this is the superimposed contribution of the PEO−PU phase. Simulated fits using the UPL equation revealed two relaxation times (τ_{PEO-PU}, τ_{PAN}) related to ionic hopping in the PEO−PU and PAN phases in addition to the conductivity relaxation time (τ_{peak}) determined from the Debye peaks. The respective power law exponents ($n_{PEO-PU} \sim 0.5-0.8$, $n_{PAN} \sim 1.0-1.6$) indicate that though cationic hopping in the softer PEO−PU phase is favored, anionic hopping in the PAN phase contributes significantly to the charge transport processes in these semi-IPNs. Correlation of the experimental results with the simulated fits enable us to distinguish the effects of semi-IPN composition, temperature, morphology, ion−ion, and ion−polymer interactions, which influence the microscopic molecular events, involved in the charge transport in these complex semi-IPN polymer electrolytes.

1. Introduction

Polymer−salt complexes have been the subject of intense investigations for the last few decades, ever since Wright[1] and Armand[2] put forward the concept of their use as solid polymer electrolytes (SPEs). Thereafter, several studies have been directed toward improving the matrix property of the host polymers and understanding the mode of ion conduction in such highly disordered systems.[3−23] Ionic conductivity in these systems occurs primarily in the amorphous regions and is associated with both the charge migration of ions between coordination sites (ionic hopping) and the polymeric chain segmental motions (micro-Brownian motions). The dynamic bond percolation theory developed by Ratner et al.[5,13,24] explains the charge migration in such systems in terms of a renewal of hopping probabilities. Monte Carlo (MC) simulations and the molecular dynamic (MD) approach on both crystalline and amorphous PEO−salt complexes have helped in establishing theoretical models to explain the mechanism responsible for ionic conductivity.[25−30] Furukawa et al.,[31,32] while making use of a combination of theoretical modeling and accurate measurements of complex conductivity spectra for PPO/$(LiClO_4)_x$ complexes, proposed that the conductivity takes place via two phenomena. The first one at high frequencies, associated with dielectric relaxations due to dipolar motions is caused by the segmental and normal-mode dynamics of the polymer host, and the second, observed at lower frequencies is the contribution from the local ionic motions. Further, experimental evidence put forth by Di Noto et al.[33−36] applies a combined approach based on universal power law (UPL) and equivalent circuit (EC) analysis on (PEG400)/$(LiCl)_x$ and (PEG400)/$(MgCl_2)_x$ polymer electrolytes.

We have successfully demonstrated the viability of a new class of PEO−PU/PVP and PEO−PU/PAN interpenetrating polymer network (IPN) salt complexes as SPEs.[37−39] These materials show superior dimensional, thermal and mechanical stability suitable for use at ambient condition. The temperature-dependent dc studies on PEO−PU/PAN/$LiClO_4$ and PEO−PU/PAN/$LiCF_3SO_3$ semi-IPNs revealed a thermally activated ion

† IICT Communication No.: 040313.

* To whom correspondence should be addressed. E-mail: manorama@iict.res.in. Phone: 91-40-27160921. FAX: 91-40-27160921.

10.1021/jp0460792 CCC: $30.25
Published on Web 12/30/2004

transport process along with a Arrhenius to VTF type of transition around the melting temperature of poly(ethylene oxide) segments.[38,39]

The primary objective of the present study put forth in this paper is to enhance our understanding of (i) the microscopic molecular events related to the charge transport mechanism, (ii) the correlated motions of the ions and chain dynamics, (iii) the identification of the polarization mechanisms and the relaxation processes, and (iv) the effect of microphase separation on such events in these semi-IPN systems. We anticipate that such a detailed analysis will aid us in the appropriate designing of the semi-IPNs as an efficient SPE for applications such as in batteries that we envisage. In contrast to earlier reports[31−36] where in low molecular weight polymers below the entanglement limits were used, the semi-IPNs investigated in the present study pose a challenge owing to their inherent complexity. The present effort is an attempt toward explaining the charge transport mechanism making use of the models proposed by Furukawa and Di Noto by suitably modifying them to account for the complexities in a semi-IPN. This paper reports simultaneous analysis of the dielectric parameters for PEO−PU/PAN/$LiClO_4$ and PEO−PU/PAN/$LiCF_3SO_3$ semi-IPNs. Initial analysis of the complex plane and spectroscopic plots strongly indicate that the composition, temperature, morphology, ion−ion, and ion−polymer interactions influence the electrical behavior of these semi-IPNs. The complete interpretation of the conductivity dispersion data obtained from impedance spectroscopy in relation to temperature and composition was achieved on the basis of Jonscher's universal power law (UPL) in the framework of the jump-relaxation model.[40−42] Correlation of these results with the structural determination previously reported by us[38,39] allowed us to propose a common conductivity mechanism for the semi-IPNs.

2. Experimental Section

2.1. Materials. Castor oil (BSS grade), diphenylmethane diisocyanate (MDI) (Ind-ital Chem. Ltd.), poly(ethylene glycol) (PEG, MW = 4000), *N*,*N*-dimethylaniline (DMA) (SD Fine Chemicals), acrylonitrile (SRL), benzoyl peroxide, acetonitrile, and tetrahydrofuran (Ranbaxy) were used as obtained. Lithium perchlorate ($LiClO_4$) prepared as reported in ref 38 and lithium triflate ($LiCF_3SO_3$) (Aldrich) were dried overnight in a vacuum at 90 °C and stored in a desiccator under nitrogen. The two classes of solvent free semi-IPN polymer electrolytes, PEO−PU/PAN/$LiClO_4$ and PEO−PU/PAN/ $LiCF_3SO_3$ were synthesized as described in refs 38 and 39. Polymer electrolytes with EO/Li mole ratios 100, 60, 30, 20, 15, and 10 were thus synthesized. The samples are coded in order of the PEO−PU/PAN weight ratio followed by the EO/Li ratio of the respective salt (for example, 60/40/ $LiClO_4$-100 corresponds to PEO−PU/PAN semi-IPN of weight ratio 60/40 doped with lithium perchlorate at EO/Li ratio = 100). The detailed characterization with respect to the thermal, mechanical, and dc properties of these semi-IPN systems are reported in ref 38 and 39.

2.2. Instrumentation. ac impedance measurements were carried out in the pre-selected intervals of frequencies between 42 Hz to 5 MHz on a computer interfaced HIOKI 3532−50 LCR HiTESTER (Hioki E. E. Corp., Japan). The disk-shaped films were sandwiched between two spring-loaded platinum blocking electrodes each of surface area 0.79 cm^2. The sample holder was placed in a thermostat-controlled heating chamber in an inert atmosphere and shielded from external electrical disturbance. The temperature was measured with an accuracy better than ±0.2 °C using a platinum−rhodium thermocouple.

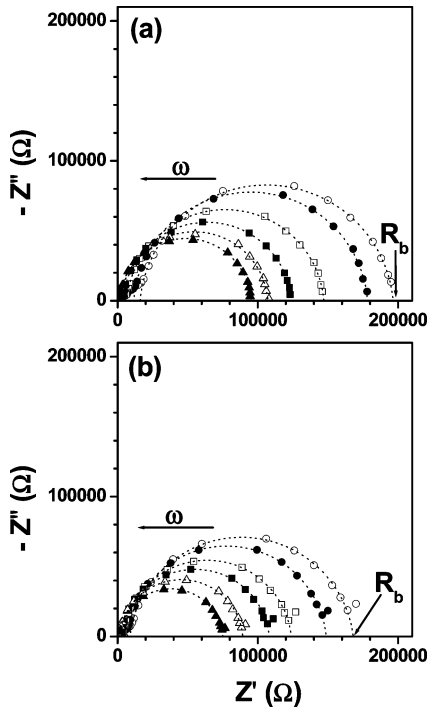

Figure 1. Complex plane plots obtained over the frequency range of 42 Hz to 5 MHz for (a) PEO−PU/PAN/$LiClO_4$-15 and (b) PEO−PU/PAN/$LiCF_3SO_3$-15 semi-IPN systems at various temperatures (○) 35 °C, (●) 40 °C, (□) 50 °C, (■) 60 °C, (△) 70 °C, and (▲) 80 °C. The dotted lines represent the simulated fits to the experimental data.

The measurements were taken in the temperature range 35−80 °C during the cooling cycle at an interval of 5 °C. The sample thickness was measured using a screw gauge and no correction for thermal expansion was taken into account. Impedance values were determined from the parallel capacitance (C_p) and conductance (G_p) data collected at each frequency by averaging five measurements. Analysis of the complex impedance data was done by nonlinear least-squares fits (NLSF) using Microcal Origin 6.0 software. The maximum error associated with the simulated fits for the universal power law equation is within ±5%.

Transmission electron microscopy (TEM) studies of the semi-IPNs were carried out on a JEOL-JEM 100CX microscope. Films of ∼0.05 μm thickness were solvent casted and lifted on copper grids for the analysis.

3. Results and Discussion

3.1. Impedance Spectroscopy Studies. Impedance spectroscopy is a powerful probe to study the structure−conductivity correlations in glassy or polymeric materials.[43] The measured parallel conductance (G_p) and capacitance (C_p) data were converted using appropriate geometric factors to determine the real and imaginary components of the dielectric permittivity (ϵ) and impedance (Z) values, respectively, for the frequency range studied. Initial studies were performed by analyzing the impedance spectra as a function of temperature and composition. Parts a and b of Figure 1 shows selected Nyquist plots for PEO−PU/PAN/$LiClO_4$ and PEO−PU/PAN/$LiCF_3SO_3$ semi-IPN systems. The data were analyzed for the temperature range 35−80 °C at an interval of 5 °C over the frequency range 42 Hz to 5 MHz for all the compositions. In the frequency window studied, spikes attributed to the diffusion-limited Warburg impedances[43] are not clearly identified at lower frequencies. However, a careful inspection of the complex-plane plots in

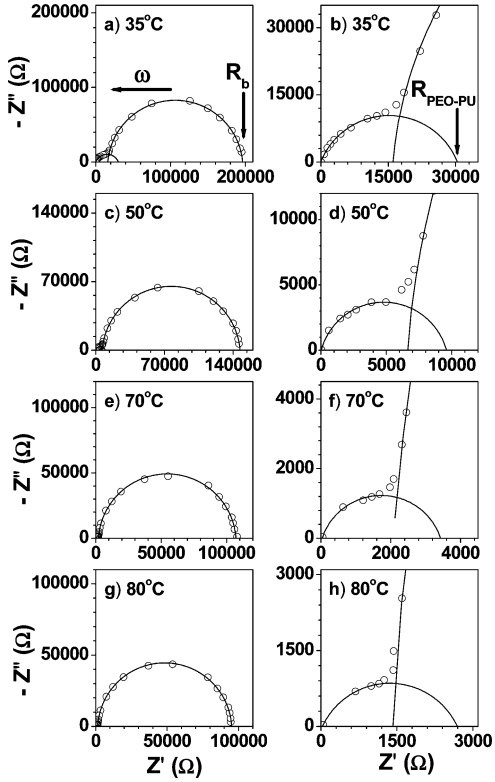

Figure 2. Complex plane plots obtained over the frequency range of 42 Hz to 5 MHz for PEO−PU/PAN/$LiClO_4$-15 semi-IPN at various temperatures (a, c, e, g) and their corresponding magnified plots of the high-frequency region showing the presence of an additional arc (b, d, f, h) attributed to the contribution from the PEO−PU phase. The solid lines represent the simulated fits to the experimental data.

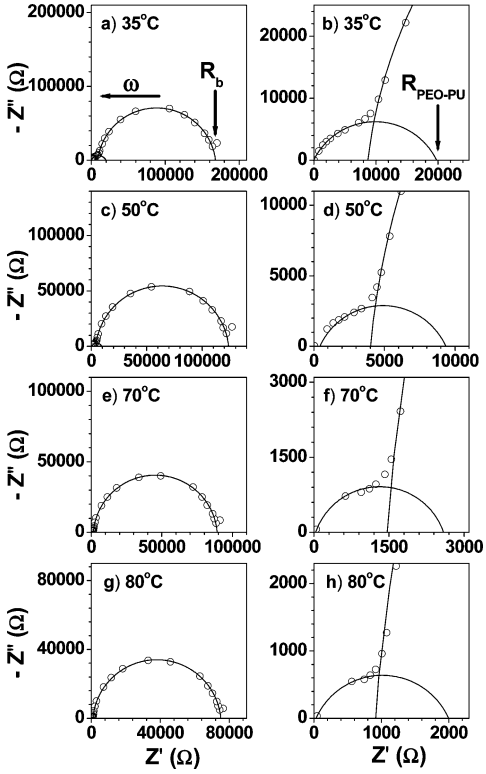

Figure 3. Complex plane plots obtained over the frequency range of 42 Hz to 5 MHz for PEO−PU/PAN/$LiCF_3SO_3$-15 semi-IPN at various temperatures (a, c, e, g) and their corresponding magnified plots of the high-frequency region showing the presence of an additional arc (b, d, f, h) attributed to the contribution from the PEO−PU phase. The solid lines represent the simulated fits to the experimental data.

the mid and high-frequency ranges reveals two well-defined and depressed semicircular arcs for all the samples throughout the temperature range of study. Representative complex plane plots for PEO−PU/PAN/$LiClO_4$ and PEO−PU/PAN/$LiCF_3SO_3$ semi-IPN systems at various temperatures are separately shown in Figures 2 and 3, respectively, to clearly emphasize the presence of the two semicircular arcs. To a first approximation, a pair of parallel RC elements in series can represent this type of profile. This conforms to a direct electrical spectroscopic signature toward the existence of two distinct microphase separated domains with dissimilar conductivities in the PEO−PU/PAN semi-IPN matrix. Several studies reported in the literature attribute the sample inhomogeneity with respect to the crystalline and amorphous regions as being responsible for this kind of behavior.[5] Nevertheless, this argument can be unambiguously ruled out in the present case of PEO−PU/PAN semi-IPNs. Justification for this comes from our earlier studies on the thermal properties of these semi-IPNs by differential scanning calorimetry (DSC).[38,39] The DSC thermograms revealed that the semi-IPNs with low salt content show a distinct morphological transition from semicrystalline to completely amorphous matrix around 55 °C (328 K). Moreover, in the case of semi-IPNs with higher amount of lithium salts the crystalline melting peak (T_m) was absent, indicating a completely amorphous matrix. Because Figures 2 and 3 clearly show the presence of both the semicircular arcs even above the crystalline melting temperature, they have been assigned to the PEO−PU and PAN phases with dissimilar conductivities on the basis of the assumption that in PEO−PU/PAN semi-IPNs the PAN component forms segregated nano-domains in the PEO−PU matrix. It is well documented in the literature that similar to poly(ethylene oxide), poly(acrylonitrile) also has the ability to solvate a variety of alkali metal salts which make them ionically conducting.[1−6,44−48] However, the PEO−PU component offers least resistance to the ionic motion presumably due to the low glass transition temperature and thereby faster chain dynamics. The low impedance semicircle (higher frequency region) is, therefore, attributed to the PEO−PU phase whereas the high impedance semicircle (lower frequency region) is attributed to the PAN phase. Figure 4 shows the transmission electron micrograph of a PEO−PU/PAN (60/40) semi-IPN system. The spherical domains of poly(acrylonitrile) with size ranging from 50 to 200 nm are clearly visible in the PEO−PU matrix which lends further support to the above assignment. This morphology is typical for two component IPNs, where one of the component undergoes nucleation and growth during the process of formation.[49]

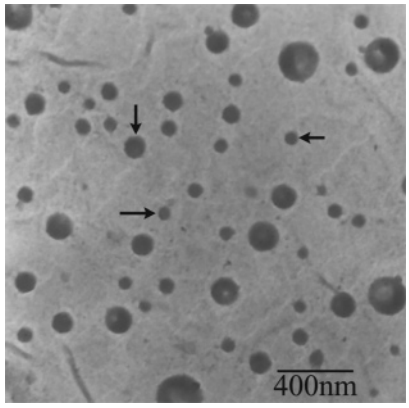

Figure 4. Transmission electron micrograph of PEO−PU/PAN semi-IPN (60/40). The arrows show the poly(acrylonitrile) phase distributed in the poly(ethylene oxide)−polyurethane matrix.

TABLE 1: Calculated Values of Resistance Obtained from the Complex-Plane Plots in the PEO−PU Phase (R_{PEO-PU}), PAN Phase (R_{PAN}), and the Bulk Resistance (R_b), along with the Capacitance in the PEO−PU Phase (C_{PEO-PU}) and PAN Phase (C_{PAN}) of the PEO−PU/PAN/$LiClO_4$ and PEO−PU/PAN/$LiCF_3SO_3$ Semi-IPN Systems at 35 °C

semi-IPN system	R_{PEO-PU} (Ω)	R_{PAN} (Ω)	R_b (Ω)	C_{PEO-PU} (F)	C_{PAN} (F)
60/40/$LiClO_4$-100	1.08×10^5	2.69×10^5	3.14×10^5	8.57×10^{-11}	3.89×10^{-10}
60/40/$LiClO_4$-60	9.87×10^4	2.41×10^5	2.98×10^5	1.02×10^{-10}	4.57×10^{-10}
60/40/$LiClO_4$-30	5.15×10^4	2.08×10^5	2.36×10^5	1.07×10^{-10}	5.39×10^{-10}
60/40/$LiClO_4$-20	3.32×10^4	1.99×10^5	2.22×10^5	1.27×10^{-10}	6.09×10^{-10}
60/40/$LiClO_4$-15	3.06×10^4	1.80×10^5	1.97×10^5	1.53×10^{-10}	5.78×10^{-10}
60/40/$LiClO_4$-10	2.32×10^4			6.48×10^{-11}	
60/40/$LiCF_3SO_3$-100	2.03×10^6			5.00×10^{-11}	
60/40/$LiCF_3SO_3$-60	1.38×10^5	3.27×10^5	3.52×10^5	6.26×10^{-11}	5.33×10^{-10}
60/40/$LiCF_3SO_3$-30	4.05×10^4	2.36×10^5	2.61×10^5	7.33×10^{-11}	5.77×10^{-10}
60/40/$LiCF_3SO_3$-20	3.31×10^4	2.02×10^5	2.16×10^5	1.18×10^{-10}	5.98×10^{-10}
60/40/$LiCF_3SO_3$-15	1.97×10^4	1.59×10^5	1.68×10^5	1.35×10^{-10}	6.94×10^{-10}
60/40/$LiCF_3SO_3$-10	4.13×10^4	2.34×10^5	2.51×10^5	1.05×10^{-10}	5.99×10^{-10}

The experimental data points obtained for both the $LiClO_4$ and $LiCF_3SO_3$ doped semi-IPN systems are simulated using nonlinear least-squares fits for semicircle (Figures 1−3). The two intercepts on the real axis correspond to the individual phase resistances (R_{PEO-PU}, R_{PAN}) and the sum corresponds to the bulk resistance (R_b) of the polymer electrolytes (PE). The errors associated with the determined parameters were within ±5%. The resulting resistances were used to determine the conductivity of the PEs at different temperatures. At the frequency corresponding to the maximum of the semicircle, ω_{max}, the magnitude of the impedance of the resistor and capacitor are equal. Thus, the values corresponding to the capacitance of the individual phases were obtained at the condition, $\omega_{max}RC = 1$.[43] The calculated R_{PEO-PU}, R_{PAN}, R_b, C_{PEO-PU}, and C_{PAN} values at 35 °C are summarized in Table 1. With an increase in temperature and salt concentration in both the systems, the conductivity of the individual phases as well as the bulk conductivity increases steadily up to a critical salt concentration (C_c). Both trends are accounted for on the basis of an increase in the number of charge carriers and faster chain dynamics, which is in agreement with our earlier studies on these electrolytes.[38,39] Above C_c, the metal ion mediated pseudo-cross-links that are formed, restrict the segmental mobility, which manifests itself as a reduced conductivity in the polymer electrolytes. These measurements strongly indicate that the composition, temperature, morphology, ion−ion, and ion−polymer interactions influence the frequency range and the shape of the Nyquist profiles.

Typical spectroscopic plots for the real part of the dielectric permittivity (ϵ') at different temperatures for the PEO−PU/PAN/$LiClO_4$ and PEO−PU/PAN/$LiCF_3SO_3$ semi-IPN systems are shown in Figure 5a,b. In the ϵ' profiles, two regions can be clearly distinguished, which suggests the presence of two different polarization processes. At high frequencies, due to the faster periodic reversal of the field, the contribution of the charge carriers (ions) toward the dielectric constant is low. In the mid-frequency range (3−300 kHz), a substantial rise in ϵ' is observed which is but an artifact of space−charge polarization. Space−charge (interfacial) polarization arises whenever phases having different conductivities are present in the same material. When an electric field is applied, the charges move through the PEO−PU phase, which is a relatively more conducting phase but are interrupted as the charges come across the high resistivity PAN phase. These barriers lead to a build up of charge at the PEO−PU/PAN interface and are manifested as an enhanced polarization. The rise of ϵ' in the low-frequency region (<300 Hz) is an additional consequence of the electrode polarization. This takes place when ions are unable to exchange with the platinum blocking electrodes and pile up at the electrode−electrolyte interface.

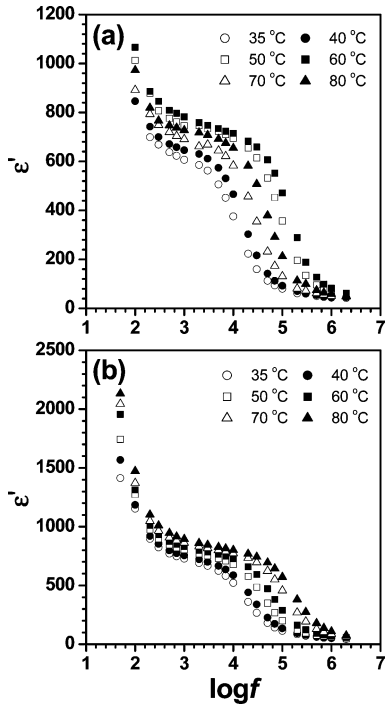

Figure 5. Frequency spectra of the real component of dielectric permittivity, $\epsilon'(\omega)$, plots of (a) PEO−PU/PAN/$LiClO_4$-15 and (b) PEO−PU/PAN/$LiCF_3SO_3$-15 semi-IPN systems at various temperatures.

The representative plots of imaginary impedance as a function of frequency (Figure 6a,b) show Lorentzian peaks that shift toward higher frequencies with an increase in temperature. The presence of these peaks is typical of Debye type relaxations occurring in the systems and depends on the composition and temperature.[43] A peak is observed when the condition $\omega\tau = 1$ is satisfied, where ω is the angular frequency and τ is the Debye relaxation time. Fitting these profiles by Lorentzian functions allows the determination of conductivity relaxation times, τ_{peak}, at the frequency corresponding to the peak maximum.

3.2. Conductivity Mechanisms. From the analysis of the complex-plane and spectroscopic plots three major inferences can be drawn: (i) ion transport in these semi-IPNs is a thermally activated process, (ii) though the semi-IPNs are highly disordered systems, the ions cannot simply be considered as "*random walkers*", but correlated motions of ions are an important characteristic of the transport mechanism, and (iii) space−charge polarization contributes significantly to the overall polarization observed in these electrolytes. It has been demonstrated that a detailed study on the frequency dependence of the real component of conductivity helps in a comprehensive understanding of the ac electrical response and the complicated ion-

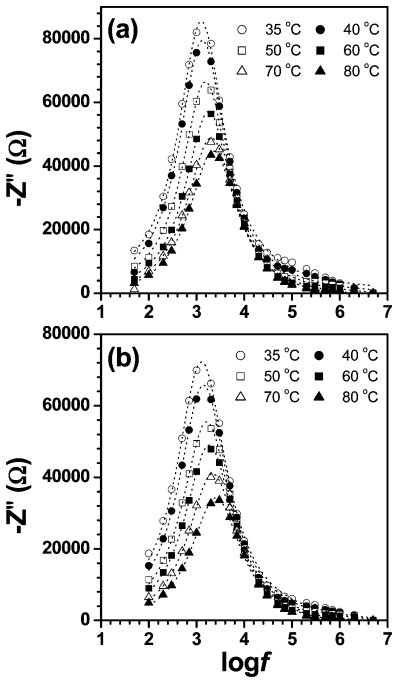

Figure 6. Imaginary component of complex impedance, $-Z'(\omega)$, versus log f plots of (a) PEO−PU/PAN/$LiClO_4$-15 and (b) PEO−PU/PAN/$LiCF_3SO_3$-15 semi-IPN systems at various temperatures. The dotted lines are the Lorentzian fits to the experimental data points.

transport mechanisms in disordered systems such as glasses and polymers.[33,50,51] The real component of conductivity, $\sigma'(\omega)$ was calculated from the impedance data using the equation[34]

$$\sigma'(\omega) = Z'(\omega)/k[(Z'(\omega))^2 + (Z''(\omega))^2] \quad (1)$$

where k is the cell constant in centimeters. Representative spectra of $\sigma'(\omega)$ profiles for the PEO−PU/PAN/$LiClO_4$ and PEO−PU/PAN/$LiCF_3SO_3$ semi-IPN systems are depicted in Figure 7a,b.

The frequency response of conductivity reflects essential features of the transport mechanisms and is found to demonstrate a high degree of universality. The conductivity is found to be almost frequency independent in the low-frequency region and is equal to the bulk conductivity (in the plateau region). Beyond a characteristic frequency ω_p, which depends on the material and temperature, the conductivity is seen to progressively increase as a function of frequency. This behavior, discussed by Jonscher is common to a wide class of materials and can be analyzed by the universal power law (UPL) equation:[40,41]

$$\sigma'(\omega) = \sigma(0) + A\omega^n \quad (2)$$

where $\sigma(0) \cong \sigma_{dc}$, the prefactor $A = \sigma(0)/(\omega_p)^n$, and n is the frequency exponent. Both $\sigma(0)$ and A are thermally activated quantities. Equation 2 can be represented by an equivalent expression:[34,35]

$$\sigma'(\omega) = \sigma(0)[1 + (\tau\omega)^n] \quad (3)$$

According to Crammer et al.,[52] τ is a time related to τ_1 where τ_1 is the initial site relaxation time of ionic hopping, $n = \tau_1/\tau^*$ is the power law exponent and τ^* is the initial back-hop relaxation time of the ionic transport process. The determination of the parameters τ and n are therefore of great significance to understand the conductivity behavior of electrolytes in terms of ion migration.

The applicability of UPL eq 3 was verified on the $\sigma'(\omega)$ profiles of both the PEO−PU/PAN/$LiClO_4$ and PEO−PU/PAN/$LiCF_3SO_3$ semi-IPN systems, using nonlinear least-squares fitting (NLSF) method. It is observed that the conductivity dispersion profiles do not obey a single power law equation throughout the frequency window studied. A prominent shoulder at high frequency (∼300 kHz) was observed for all the samples. Di Noto in his study on poly[PEG400-*alt*-DEOS]/$(MgCl_2)_x$ systems reported a similar deviation from the simple power law in the profile of conductivity dispersion data.[33] This particular spectral feature has been attributed to an additional anionic hopping event with a different relaxation time along with the normal cationic hopping process of charge migration. However, attempts to fit the generalized universal power law (G-UPL), as suggested by Di Noto, with N number of processes and considering the fractional contribution of each was also found unsuitable for these semi-IPN systems. Nevertheless, the data when treated as a superimposed profile, considering independent contribution from both the PAN and PEO−PU phases separately, obey the UPL equation appropriately. As seen in Figure 7a,b each profile has been fitted with two power law equations, where the frequency region up to ∼300 kHz is the conductivity profile of the PAN phase and beyond this is the superimposed contribution of the PEO−PU phase. From the simulated fits, two sets of fitting parameters ($\sigma(0)_{PEO-PU}$, $\sigma(0)_{PAN}$, τ_{PEO-PU}, τ_{PAN}, n_{PEO-PU}, and n_{PAN}) for each conductivity dispersion data were obtained. The fitting parameters for the PEO−PU/PAN/$LiClO_4$ and PEO−PU/PAN/$LiCF_3SO_3$ semi-IPN systems at 35 °C are listed in Table 2.

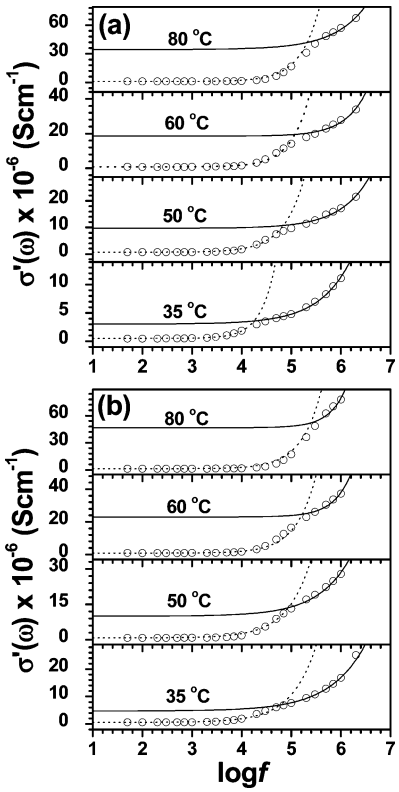

Figure 7. Real component of conductivity, $\sigma'(\omega)$, frequency spectra of (a) PEO−PU/PAN/$LiClO_4$-15 and (b) PEO−PU/PAN/$LiCF_3SO_3$-15 semi-IPN systems at various temperatures. Two separate nonlinear least-squares fitting curves using the universal power law equation, $\sigma'(\omega) = \sigma(0)[1 + (\tau_1\omega)^n]$ are obtained for the experimental data at each temperature. The dotted line represents the simulated fits to the PAN phase whereas the solid line represents the fits to PEO−PU phase.

To have a comprehensive understanding of the physical processes of charge transfer in these semi-IPN systems, the results obtained can be interpreted on the following lines. The charge migration process in a polymer electrolyte depends

TABLE 2: Parameters $\sigma(0) \cong \sigma_{dc}$, Relaxation Time ($\tau$), and Frequency Exponent (n) Obtained from the Universal Power Law Fits for the PEO−PU and PAN Phases of the PEO−PU/PAN/$LiClO_4$ and PEO−PU/PAN/$LiCF_3SO_3$ Semi-IPN Systems at 35 °C

semi-IPN system	$\sigma(0)_{PEO-PU}$ (S cm^{-1})	$\sigma(0)_{PAN}$ (S cm^{-1})	τ_{PEO-PU} (s)	τ_{PAN} (s)	τ_{peak} (s)	n_{PEO-PU}	n_{PAN}
60/40/$LiClO_4$-100	8.59×10^{-7}	3.86×10^{-7}	1.39×10^{-6}	3.0×10^{-5}	1.39×10^{-4}	0.69	1.62
60/40/$LiClO_4$-60	9.41×10^{-7}	3.45×10^{-7}	2.98×10^{-6}	4.0×10^{-5}	1.74×10^{-4}	0.54	1.23
60/40/$LiClO_4$-30	1.81×10^{-6}	4.47×10^{-7}	1.11×10^{-6}	3.0×10^{-5}	1.46×10^{-4}	0.63	1.28
60/40/$LiClO_4$-20	2.80×10^{-6}	4.66×10^{-7}	5.50×10^{-7}	4.0×10^{-5}	1.53×10^{-4}	0.78	1.34
60/40/$LiClO_4$-15	3.04×10^{-6}	5.16×10^{-7}	7.01×10^{-7}	3.0×10^{-5}	1.26×10^{-4}	0.68	1.48
60/40/$LiClO_4$-10	4.00×10^{-6}		4.17×10^{-7}			0.65	
60/40/$LiCF_3SO_3$-100	4.79×10^{-7}		2.63×10^{-6}			0.41	
60/40/$LiCF_3SO_3$-60	9.02×10^{-7}	2.84×10^{-7}	4.87×10^{-6}	3.0×10^{-5}	1.81×10^{-4}	0.53	1.04
60/40/$LiCF_3SO_3$-30	1.95×10^{-6}	3.92×10^{-7}	5.91×10^{-7}	3.0×10^{-5}	1.75×10^{-4}	0.69	1.39
60/40/$LiCF_3SO_3$-20	2.81×10^{-6}	4.59×10^{-7}	1.30×10^{-6}	4.0×10^{-5}	1.45×10^{-4}	0.57	0.94
60/40/$LiCF_3SO_3$-15	4.71×10^{-6}	5.81×10^{-7}	7.63×10^{-7}	4.0×10^{-5}	1.26×10^{-4}	0.61	0.89
60/40/$LiCF_3SO_3$-10	2.25×10^{-6}	3.98×10^{-7}	1.55×10^{-6}	5.0×10^{-5}	1.69×10^{-5}	0.61	0.95

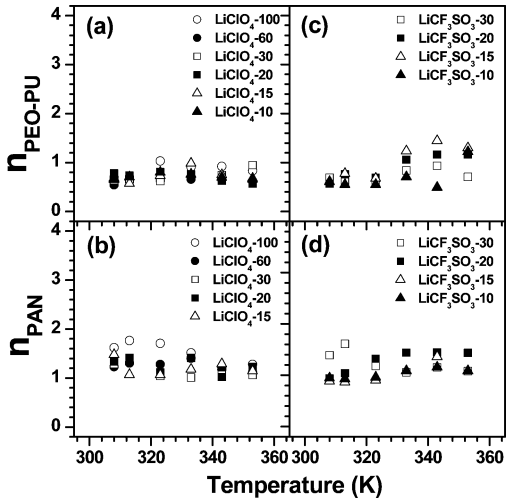

Figure 8. Plots of power law exponent, n as a function of temperature for (a) PEO−PU phase (n_{PEO-PU}), (b) PAN phase (n_{PAN}) of PEO−PU/PAN/$LiClO_4$ semi-IPNs, (c) PEO−PU phase (n_{PEO-PU}), and (d) PAN phase (n_{PAN}) of PEO−PU/PAN/$LiCF_3SO_3$ semi-IPNs

significantly on a successful hop from the sites coordinating an ion to an empty site, which could coordinate the ion. Thus the interchain hopping events in a polymer electrolyte can be physically interpreted on two distinct time scales. The first associated with the instantaneous hop and the second with the time involved in host medium reorganization.[24,53,54] The host medium reorganization can be attributed to both ionic correlation events between the polymer complex cations and anions, and the geometrical reorganization of the coordination cage, accommodating the ion after the hop. Depending on the class of polymer electrolytes, two types of interchain hopping events, classified as the cationic and anionic hopping can occur in the bulk material, both of which contribute to the overall cationic migration.[33]

The analysis of the UPL exponent n, which is the ratio of initial back hop rate ($r_b = 1/\tau^*$) to the initial site relaxation rate ($r_s = 1/\tau_1$) reveals that the conductivity due to cationic hopping event is successful when $r_s > r_b$, i.e., $n < 1$.[52] Figure 8a−d shows the variation of n_{PEO-PU} and n_{PAN} obtained from the UPL fit for PEO−PU and PAN phases of PEO−PU/PAN/$LiClO_4$ and PEO−PU/PAN/$LiCF_3SO_3$ semi-IPN systems as a function of temperature. No particular trend was observed for n_{PEO-PU} and n_{PAN} with respect to the temperature and concentration of the salt. However, n_{PAN} in both $LiClO_4$ and $LiCF_3SO_3$ doped semi-IPNs was seen to be in the range 1.0−1.6. The n_{PEO-PU} in the case of $LiClO_4$ was seen to be considerably less than 1 (in the range of 0.5−0.8), whereas for $LiCF_3SO_3$ it is around 0.5−0.8 at lower temperatures which increases to 0.8−1.2 above ∼330 K. The results indicate that in the case of $LiClO_4$ the back hop rate in the softer PEO−PU phase is lower than the initial site relaxation rate, which satisfies the condition for cationic hopping process. However, in the case of PAN phases where $n > 1$ was observed for all the samples, the back hop rate is always higher than the initial site relaxation rate. This phenomenon is possible if the cationic migration takes place through an anionic hopping mechanism.[33] During an anionic hop between the metal ion coordinated polymer sites, negligible geometrical arrangement of the sites is expected. This results in a decrease in the site relaxation rate. In the case of the $LiCF_3SO_3$ doped PEO−PU phase the cationic hopping at lower temperatures is seen to change progressively to anionic hopping at higher temperatures. Thus, it can be inferred that in the case of the PEO−PU/PAN/$LiClO_4$ and PEO−PU/PAN/$LiCF_3SO_3$ semi-IPNs, substantial contribution of anionic hopping leads to the overall charge migration.

Additional information on the conductivity mechanism in these systems is obtained by studying the conductivity relaxation times, τ_{peak}, determined from the Debye peaks and τ_{PAN} and τ_{PEO-PU} (a time correlated to the initial site relaxation time) determined from the UPL fit of the $\sigma'(\omega)$ data, respectively. τ_{PEO-PU} and τ_{PAN} associated with ionic hopping show shorter relaxation times for PEO−PU, indicating faster chain dynamics in the PEO−PU phase compared to that of PAN. The analysis of the temperature dependences of these relaxation times as presented in Figure 9 shows typical Arrhenius behavior.

$$\tau = \tau_0 \exp(-\Delta E_a/kT) \tag{4}$$

The calculated values of the preexponential factor corresponding to $\tau_{0,peak}$, $\tau_{0,PEO-PU}$, and $\tau_{0,PAN}$ along with the respective activation energy for the thermally stimulated conductivity relaxation time, $E_{a,peak}$, and site relaxation energy height barrier for the two phases ($E_{a,PEO-PU}$ and $E_{a,PAN}$) are summarized in Table 3. It is observed that $E_{a,PAN}$ is approximately equivalent to $E_{a,peak}$, suggesting that the site relaxation processes in the PAN phase coincide with the bulk conductivity relaxation process. Semi-IPNs by their very nature are highly entangled systems and hence restricts the host medium reorganization. Because both PEO−PU and PAN are conducting phases with $\sigma_{PEO-PU} > \sigma_{PAN}$, the resultant bulk conductivity is controlled by the relatively less conducting PAN phase. Thus, even though the $E_{a,PEO-PU}$ is considerably lower, the restriction of the polymer chain mobility in the bulk material due to the presence of PAN phase proves to be a determining factor in the conduction mechanism. This observation once again demonstrates that the movements of the free charge carriers as well as the polymer chain dynamics mainly regulate the conductivity in these polymer electrolytes.

3.3. Conductivity Scaling. Scaling of the ac conductivity data is a suitable tool for comparing the ion dynamics of

TABLE 3: Pre-exponential Constant (τ_0) and Activation Energy (E_a) Obtained from the Arrhenius Fits to the log τ versus 1000/T Plots for the Conductivity Relaxation Time (τ_{Peak}) and Initial Site Relaxation Times (τ_{PEO-pu}, τ_{PAN}) in PEO−PU and PAN Phases, Respectively, for the Semi-IPNs

semi-IPN system	$\tau_{0,peak}$ (s)	$\tau_{0,PEO-PU}$ (s)	$\tau_{0,PAN}$ (s)	$E_{a,peak}$ (eV)	$E_{a,PEO-PU}$ (eV)	$E_{a,PAN}$ (eV)
60/40/$LiClO_4$-100	1.45×10^{-6}	3.58×10^{-11}	5.71×10^{-7}	0.12	0.28	0.11
60/40/$LiClO_4$-60	4.05×10^{-7}	1.17×10^{-12}	4.21×10^{-7}	0.16	0.38	0.13
60/40/$LiClO_4$-30	4.69×10^{-8}	5.79×10^{-15}	9.94×10^{-8}	0.21	0.51	0.16
60/40/$LiClO_4$-20	2.33×10^{-7}	2.19×10^{-11}	2.29×10^{-7}	0.17	0.27	0.14
60/40/$LiClO_4$-15	1.37×10^{-6}	6.10×10^{-16}	5.71×10^{-7}	0.12	0.55	0.11
60/40/$LiClO_4$-10						
60/40/$LiCF_3SO_3$-100						
60/40/$LiCF_3SO_3$-60	1.31×10^{-7}	5.23×10^{-10}	5.12×10^{-7}	0.21	0.35	0.13
60/40/$LiCF_3SO_3$-30	1.56×10^{-7}	5.62×10^{-9}	8.43×10^{-7}	0.19	0.12	0.09
60/40/$LiCF_3SO_3$-20	2.49×10^{-8}	7.49×10^{-14}	6.28×10^{-11}	0.23	0.42	0.36
60/40/$LiCF_3SO_3$-15	5.54×10^{-7}	3.93×10^{-13}	4.66×10^{-9}	0.14	0.38	0.24
60/40/$LiCF_3SO_3$-10	2.55×10^{-7}	1.49×10^{-13}	1.32×10^{-8}	0.17	0.44	0.22

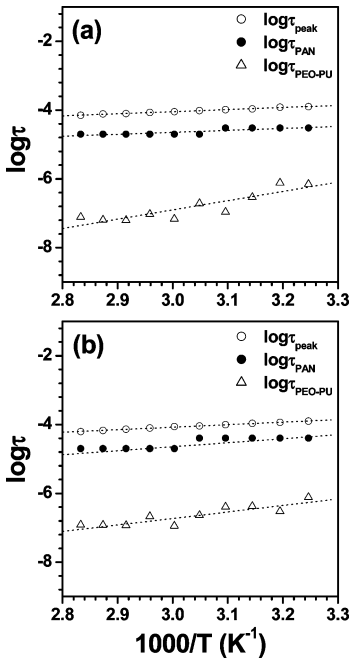

Figure 9. log τ versus 1000/T plots of conductivity relaxation time (τ_{peak}), initial site relaxation time for the PEO−PU phase (τ_{PEO-PU}), and initial site relaxation time for PAN phases (τ_{PAN}) in (a) PEO−PU/PAN/$LiClO_4$-15 and (b) PEO−PU/PAN/$LiCF_3SO_3$-15 semi-IPN systems. The dotted lines show the Arrhenius fit.

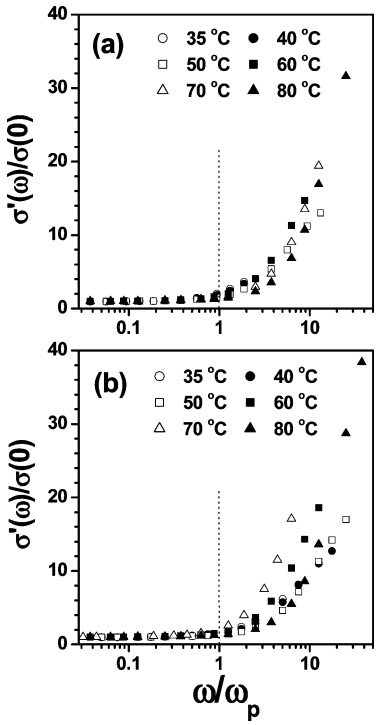

Figure 10. Scaled ac conductivity plots, $\sigma'(\omega)/\sigma(0)$, as a function of ω/ω_p for the PAN phase of (a) PEO−PU/PAN/$LiClO_4$-15 and (b) PEO−PU/PAN/$LiCF_3SO_3$-15 semi-IPN systems. Beyond $\omega/\omega_p \sim 1$, as indicated by the dotted line significant dispersion of the data is observed.

different materials.[55] The ability to scale different data sets so as to collapse all to one common master curve indicates that the process can be separated into a common physical mechanism modified only by thermodynamic scales. This is called the time−temperature superposition principle (TTSP).[55−60] Of the two approaches, viz. the Dyre's random free energy barrier model[61] and the Almond-West conductivity formalism,[61,62] the latter has been more popular, possibly due to the simplicity of the treatment. In the Almond-West formalism, the scaling behavior is obtained from eq 3 and is given by

$$\sigma'(\omega) = \sigma(0)[1 + (\omega/\omega_p)^n] \quad (5)$$

where $\omega_p = 1/\tau$ is the hopping frequency.

In this approach, the hopping frequency (ω_p) and dc conductivity, $\sigma(0)$, are used as the scaling parameters for the frequency axis and the conductivity axis, respectively.

Parts a and b of Figure 10 show the typical scaled plots for the PAN phase of PEO−PU/PAN/$LiClO_4$-15 and PEO−PU/PAN/$LiCF_3SO_3$-15 semi-IPN systems, respecively. It is observed that, though the experimental data in the low-frequency regions collapsed, there is significant dispersion in the data beyond $\omega/\omega_p = 1$. The initial collapse of the ac conductivity data in the region $\omega/\omega_p < 1$ strongly indicates that the relaxation mechanism occurring in the PAN phase is independent of the temperature. The departure beyond $\omega/\omega_p > 1$, can be well understood by taking into consideration the fact that in this region there is significant contribution from a superimposed second phase, which in this particular case is PEO−PU. Thus, contrary to the expectations of obtaining a single master curve throughout the frequency range, the $\sigma'(\omega)$ profiles of PEO−PU/PAN/$LiClO_4$ and PEO−PU/PAN/$LiCF_3SO_3$ semi-IPNs could not be scaled down. This proves our original contention about the presence of two distinct relaxation processes in the constituent PEO−PU and PAN phases in these semi-IPNs.

4. Conclusions

In this study, for the first time we have made an attempt to provide a detailed insight into the ion transport mechanisms at play in the new class of PEO−PU/PAN semi-IPN−salt complex polymer electrolytes. A simultaneous investigation on the

electrical response of two classes of PEO−PU/PAN semi-IPNs doped with $LiClO_4$ and $LiCF_3SO_3$ (EO/Li mole ratio 100, 60, 30, 20, 15, 10) has been carried out by impedance spectroscopy in the range 42 Hz to 5 MHz and over a temperature range of 35−80 °C. Preliminary analysis of the complex plane plots in the mid- and high-frequency range revealed the presence of two microscopic phases, which also gains support from the TEM studies. The low impedance arc is attributed to the PEO−PU domains and the high impedance arc to the PAN phase. Dielectric permittivity profiles suggest the contribution from both the space charge and electrode polarization to the overall polarization process.

The real part of conductivity, $\sigma'(\omega)$, spectroscopic profiles were fitted to two power law equations, where the frequency region up to ~300 kHz is the conductivity profile associated with the PAN phase and beyond this is the superimposed contribution of the PEO−PU phase. The simulated fits generated two sets of fitting parameters ($\sigma(0)_{\text{PEO−PU}}$, $\sigma(0)_{\text{PAN}}$, $\tau_{\text{PEO−PU}}$, τ_{PAN}, $n_{\text{PEO−PU}}$, and n_{PAN}) corresponding to each conductivity dispersion data. The power law exponent, n for the PAN phase in both PEO−PU/PAN/$LiClO_4$ and PEO−PU/PAN/$LiCF_3SO_3$ semi-IPN systems was found to be in the range 1.0−1.6, which indicates a higher back hop rate compared to the initial site relaxation rate. This suggests that anionic hopping results in the cation migration without any substantial geometrical site relaxation in this phase. The $n_{\text{PEO−PU}}$ was in the range of 0.5−0.8 for $LiClO_4$ complexes whereas for $LiCF_3SO_3$, the n value increased slightly to 0.8−1.2 above ~330 K. This indicates that in PEO−PU phase the ionic migration is predominantly due to cationic hopping. Even though cationic hopping is favored in the softer PEO−PU phase, anionic hopping in the PAN phase contributes significantly to the overall cation migration in these semi-IPNs. $\tau_{\text{PEO−PU}}$ and τ_{PAN} associated with ionic hopping shows shorter relaxation times for the PEO−PU phase, which indicates faster chain dynamics in this phase compared to that of PAN. Moreover, from the Arrhenius fits of the temperature dependence of relaxation times it was observed that $E_{\text{a,PAN}}$ was found approximately equivalent to $E_{\text{a,peak}}$. These results suggest that in PEO−PU/PAN semi-IPNs, the comparatively rigid PAN phase, which restricts the overall polymer segmental chain mobility becomes the determining factor in the conduction mechanism. Thus, a suitably modified approach based on UPL considering the independent contribution from the individual microphases of the semi-IPNs enabled a complete interpretation of the microscopic molecular events related to the charge transports in these complex semi-IPN polymer electrolytes.

In summary, the results presented in this paper demonstrate that the overall electrical behavior of the investigated semi-IPN polymer electrolytes depends on the composition, temperature, migrating ionic species, ion−ion and ion−polymer interactions, morphology of the matrix, and the polymer chain dynamics.

Acknowledgment. We thank Dr. Shashi Singh, Scientist, CCMB, Hyderabad, India for recording the electron micrographs. P.B. acknowledges "Council of Scientific and Industrial Research", India for financial assistance in the form of a senior research fellowship (SRF).

Supporting Information Available: Individual complex plane plots obtained at different temperatures for PEO−PU/PAN/$LiClO_4$ and PEO−PU/PAN/$LiCF_3SO_3$ semi-IPNs with various EO/Li mole ratios and more detailed plots of $\sigma'(\omega)$ frequency spectra shown in Figure 7 are provided. This material is available free of charge via the Internet at http://pubs.acs.org.

References and Notes

(1) Fenton, D. E.; Parker, J. M.; Wright, P. V. *Polymer* **1973**, *14*, 589.
(2) Armand, M. *Solid State Ionics* **1983**, *9*−*10*, 745.
(3) Ratner, M. A.; Shriver, D. F. *Chem. Rev.* **1988**, *88*, 109.
(4) Gray, F. M. *Solid Polymer Electrolytes*; VCH: NewYork, Weinheim, Germany, 1991.
(5) MacCallum, J. R.; Vincent, C. A. *Polymer Electrolyte Reviews-1*; Elsevier Applied Science Edition: London, U.K., 1987; Vol. 1, p 351.
(6) Eisenberg, A.; Ovans, K.; Yoon, H. N. In *Ions in Polymers*; A. Eisenberg, Ed.; Advances in Chemistry Series 187; American Chemical Society: Washington, DC, 1980; p 267.
(7) Mertens, J. A.; Wubbenhorst, M.; Oosterbaan, W. D.; Jenneskens, L. W.; van Turnhout, J. *Macromolecules* **1999**, *32*, 3314.
(8) Allcock, H. R.; Napierala, M. E.; Cameron, C. G.; O'Connor, S. J. M. *Macromolecules* **1996**, *29*, 1951.
(9) Cowie, M. G.; Cree, S. H. *Annu. Rev. Phy. Chem.* **1989**, *40*, 85.
(10) Allcock, H. R.; Sunderland, H. J.; Ravikiran, R.; Nelson, J. M. *Macromolecules* **1998**, *31*, 8026.
(11) Jean-Franois, N.; Alessandro, G.; Cheradame, H.; Jean-Pierre, C. A. *Macromolecules* **1988**, *21*, 1117.
(12) Hawker, C. J.; Chu, F.; Pomery, P. J.; Hill, D. J. T. *Macromolecules* **1996**, *29*, 3831.
(13) Druger, S. D.; Nitzan, A.; Ratner, M. *J. Chem. Phys.* **1983**, *79*, 3133.
(14) Shi, J.; Vincent, C. A. *Solid State Ionics* **1993**, *60*, 11.
(15) Andreev, Y. G.; Bruce, P. G. *Electrochim. Acta* **2000**, *45*, 1417.
(16) Li, J.; Pratt, L. M.; Khan, I. M. *J. Polym. Sci., Part A: Polym. Chem. Ed.* **1995**, *33*, 1657.
(17) Acosta, J. L.; Enrique, M. *J. Appl. Polym. Sci.* **1996**, *60*, 1185.
(18) Munichandraiah, N.; Sivasankar, G.; Scanlon, L. G.; Marsh, R. A. *J. Appl. Polym. Sci.* **1997**, *65*, 2191.
(19) Watanabe, M.; Sanui, K.; Ogata, N.; Kobayashi, T.; Ohtaki, Z. *J. Appl. Phys.* **1985**, *57*, 123.
(20) Florjanczyk, Z.; Krawiec, W.; Wieczorek, W.; Siekierski, M. *J. Polym. Sci., Part B: Polym. Phys. Ed.* **1995**, *33*, 629.
(21) Allcock, H. R.; O'Connor, S. J. M.; Olmeijer, D. L.; Napierala, M. E.; Cameron, C. G. *Macromolecules* **1996**, *29*, 7544.
(22) Zhang, Z.; Fang, S. *J. Appl. Polym. Sci.* **2000**, *77*, 2957.
(23) Ichikawa, K.; Dickinson, L. C.; MacKnight, W. J.; Watanabe, M.; Ogata, N. *Polymer* **1992**, *33*, 4699.
(24) Druger, S. D.; Ratner, M. A.; Nitzan, A. *Phys. Rev. B* **1985**, *31*, 3939.
(25) Neyertz, S.; Brown, D.; Thomas, J. O. *J. Chem. Phys.* **1994**, *101*, 10064.
(26) Neyertz, S.; Brown, D.; Thomas, J. O. *Electrochim. Acta* **1995**, *40*, 2063.
(27) Neyertz, S.; Brown, D. *J. Chem. Phys.* **1995**, *102*, 9275.
(28) Lin, B.; Boinske, P. T.; Halley, J. W. *J. Chem. Phys.* **1996**, *105*, 1668.
(29) Smith, G. D.; Yoon, D. Y.; Jaffe, R. L.; Colby, R. H.; Krishnamoorti, R.; Fetters, L. J. *Macromolecules* **1996**, *29*, 3462.
(30) Hyun, J. K.; Dong, H.; Rodes, C. P.; Frech, R.; Wheeler, R. A. *J. Phys. Chem. B* **2001**, *105*, 3329.
(31) Furukawa, T.; Imura, M.; Yuruzume, H. *Jpn. J. Appl. Phys.* **1997**, *36*, 1119.
(32) Furukawa, T.; Yoneya, K.; Takahashi, Y.; Ito, K.; Ohno, H. *Electrochim. Acta* **2000**, *45*, 1443.
(33) Di Noto, V. *J. Phys. Chem. B* **2002**, *106*, 11139.
(34) Di Noto, V.; Vittadello, M.; Lavina, S.; Fauri, M.; Biscazzo, S. *J. Phys. Chem. B* **2001**, *105*, 4584.
(35) Di Noto, V.; Vittadello, M. *Solid State Ionics*, **2002**, *147*, 309.
(36) Di Noto, V. *J. Phys. Chem. B* **2000**, *104*, 10116.
(37) Basak, P.; Parkash, O.; Chatterji, P. R. *J. Macromol. Sci-Pure Appl. Chem.* **2001**, *A38*, 399.
(38) Basak, P.; Manorama, S. V. *Solid State Ionics* **2004**, *167*, 113.
(39) Basak, P.; Manorama, S. V. *Eur. Polym. J.* **2004**, *40*, 1155.
(40) Jonscher, A. K. *Nature* **1977**, *267*, 673.
(41) Jonscher, A. K. *Dielectric Relaxation in Solids*; Chelsea Dielectrics: London, 1983.
(42) Funke, K. *Z. Phys. Chem.* **1995**, *188*, 243.
(43) MacDonald, J. R.; Johnson, W. B. In *Impedance Spectroscopy*; MacDonald, J. R., Ed.; J. Wiley & Sons: NewYork, 1987; p 23.
(44) Watanabe, M.; Kanba, M.; Nagaoka, K. *J. Polym. Sci.* **1983**, *21*, 939.
(45) Abraham, K. M.; Alamgir, M. *J. Electrochem. Soc.* **1990**, *136*, 1657.
(46) Forsyth, M.; Sun, J.; MacFarlan, D. R. *Solid State Ionics* **1998**, *112*, 161.
(47) Forsyth, M.; Sun, J.; MacFarlan, D. R.; Hill, A. J. *J. Polym. Sci., Polym. Phys.* **2000**, *38*, 341.
(48) Perera, K.; Dissanayake, M. A. K. L.; Bandaranayake, P. W. S. K. *Electrochim. Acta* **2000**, *45*, 1361.
(49) Sperling, L. H. In *Interpenetrating Polymer Networks*, Klempner, D.; Sperling, L. H.; Utrachi, L. A., Eds.; Advances in Chemistry Series 239; American Chemical Society: Washington, DC, 1994; p 3.

(50) Roling, B.; Martiny, C.; Funke, K. *J. Non-Cryst. Solids* **1999**, *249*, 201.
(51) Roling, B. *J. Non-Cryst. Solids* **1999**, *244*, 34.
(52) Cramer, C.; Funke, K.; Seatkamp, T.; Wilmer, D.; Ingram, M. D. *Naturforsch. A* **1995**, *50*, 613.
(53) Lonergan, M. C.; Perram, J. W.; Ratner, M.; Shriver, D. F. *J. Chem. Phys.* **1993**, *98*, 4937.
(54) Lonergan, M. C.; Nitzan, A.; Ratner, M.; Shriver, D. F. *J. Chem. Phys.* **1995**, *103*, 3253.
(55) Roling, B.; Happe, A.; Funke, K.; Ingram, M. D. *Phys. Rev. Lett.* **1997**, *78*, 2160.
(56) Elliott, S. R. *Solid State Ionics* **1994**, *70*−*71*, 27.
(57) Ghosh, A.; Pan, A. *Phys. Rev. Lett.* **2000**, *84*, 2188.
(58) Sidebottom, D. L. *Phys. Rev. Lett.* **1999**, *82*, 3653.
(59) Roling, B. *Solid State Ionics* **1998**, *105*, 185.
(60) Schroder, T. B.; Dyre, J. C. *Phys. Rev. Lett.* **2000**, *84*, 310.
(61) Almond, D. P.; West, A. R. *Solid State Ionics* **1987**, *23*, 27.
(62) Almond, D. P.; West, A. R. *Solid State Ionics* **1983**, *9*−*10*, 277.